Projected Changes in Extreme High Temperature and Heat Stress in China

Xingcai LIU[1], Qiuhong TANG[1,2*], Xuejun ZHANG[1], and Siao SUN[3]

1 *Key Laboratory of Water Cycle and Related Land Surface Processes, Institute of Geographic Sciences and Natural Resources Research, Chinese Academy of Sciences, Beijing* 100101
2 *University of Chinese Academy of Sciences, Beijing* 100049
3 *Key Laboratory of Regional Sustainable Development Modeling, Institute of Geographic Sciences and Natural Resources Research, Chinese Academy of Sciences, Beijing* 100101

(Received August 9, 2017; in final form March 21, 2018)

ABSTRACT

High temperature accompanied with high humidity may result in unbearable and oppressive weather. In this study, future changes of extreme high temperature and heat stress in mainland China are examined based on daily maximum temperature (T_x) and daily maximum wet-bulb globe temperature (T_w). T_w has integrated the effects of both temperature and humidity. Future climate projections are derived from the bias-corrected climate data of five general circulation models under the Representative Concentration Pathways (RCPs) 2.6 and 8.5 scenarios. Changes of hot days and heat waves in July and August in the future (particularly for 2020–50 and 2070–99), relative to the baseline period (1981–2010), are estimated and analyzed. The results show that the future T_x and T_w of entire China will increase by 1.5–5°C on average around 2085 under different RCPs. Future increases in T_x and T_w exhibit high spatial heterogeneity, ranging from 1.2 to 6°C across different regions and RCPs. By around 2085, the mean duration of heat waves will increase by 5 days per annum under RCP8.5. According to T_x, heat waves will mostly occur in Northwest and Southeast China, whereas based on T_w estimates, heat waves will mostly occur over Southeast China and the mean heat wave duration will be much longer than those from T_x. The total extreme hot days (T_x or T_w > 35°C) will increase by 10–30 days. Southeast China will experience the severest heat stress in the near future as extreme high temperature and heat waves will occur more often in this region, which is particularly true when heat waves are assessed based on T_w. In comparison to those purely temperature-based indices, the index T_w provides a new perspective for heat stress assessment in China.

Key words: high temperature, wet-bulb globe temperature, heat stress, climate change

Citation: Liu, X. C., Q. H. Tang, X. J. Zhang, et al., 2018: Projected changes in extreme high temperature and heat stress in China. *J. Meteor. Res.*, **32**(3), 351–366, doi: 10.1007/s13351-018-7120-z.

1. Introduction

High temperature extremes in summer have been increasingly reported in many areas of the world (Schar et al., 2004; Barriopedro et al., 2011; Hauser et al., 2016; Sun et al., 2016) and have caused considerable socioeconomic damage (Sun et al., 2014) and health issues. For instance, thousands of excess deaths and a number of wildfires were reported during the heat wave in summer 2003 in Europe (Grazzini et al., 2003). China has been frequently struck by heat waves, wherein many areas suffered record-breaking heat in recent years (e.g., the extremely hot summer of 2015; Miao et al., 2016; Sun et al., 2016). Sun et al. (2014) showed that in eastern China the strongest heat waves during the past several decades mostly occurred after 2000. It was reported that the number of heat waves had significantly increased (Mishra et al., 2015) and the historical extreme heat waves were projected to become the norm in the future in many regions of the world (Mueller et al., 2016).

Pure temperature indices (e.g., daily maximum temperature) have been widely used to characterize heat events in terms of magnitude and duration. Characteristics of extreme heat events in China have been well docu-

Supported by the National Natural Science Foundation of China (41730645 and 41425002), Key Research Program of the Chinese Academy of Sciences (ZDRW-ZS-2017-4), National Youth Top-Notch Talent Support Program in China, and Chinese Postdoctoral Science Foundation (2016M601117).

*Corresponding author: tangqh@igsnrr.ac.cn.

mented in numerous studies focusing on extreme high temperatures and hot days (e.g., Yan et al., 2002; Zhai and Pan, 2003; Qi and Wang, 2012; You et al., 2014). Recent studies showed that the current high risk of heat waves in China would continue and might increase in the future (Leng et al., 2016; Guo et al., 2017; Li et al., 2017; Zhang et al., 2017). However, pure temperature indices can hardly represent the apparent temperature (temperature equivalent perceived by humans) because human comfort is not only affected by the exposure to temperature but also affected by other ambient conditions such as humidity and wind. For example, high ambient temperature and humidity may reduce the evaporative cooling effect and the heat conduction on the human body, and consequently increase mortality as well as morbidity (Fischer and Knutti, 2013). The heat stress index that combines temperature and humidity such as apparent temperature (Steadman, 1979) can provide a closer approximation of thermal comfort of humans in comparison of the use of temperature alone, and is thus increasingly used to address health impact on humans (e.g., Mitchell, 2016; Wehner et al., 2016). The wet-bulb globe temperature (WBGT) derived from several observed metrics such as the wet-bulb temperature, the globe temperature, and the dry-bulb (ambient air) temperature, was also a most widely used index of heat stress (Budd, 2008). To overcome the data limitation, both the apparent temperature (Steadman, 1984) and the WBGT (Willett and Sherwood, 2012) were simplified to approximate the heat stress index by using regular meteorological data (e.g., temperature, humidity, and water vapor pressure), which makes it possible for assessment of changes in heat stress at large scales.

Heat stress assessment in China considering both temperature and humidity has been reported for certain historical periods (e.g., Wang and Gaffen, 2001; Ding and Qian, 2011; Chen and Li, 2017; You et al., 2017). Li et al. (2017) assessed the spatiotemporal characteristics of heat waves in China by using a compound heat wave index defined by daily maximum and minimum temperature; the compound index used to some degree addressed the health impact of heat wave events. However, future heat stress projection in China by using the WBGT has not been assessed so far. Compared with purely temperature-based indices, the WBGT is advantageous in providing more integrated quantification of climate impacts on heat stress (i.e., the climate impacts with respect to human health), and its projections in climate models show less uncertainties than independent temperature estimates (Fischer and Knutti, 2013). Therefore, a comprehensive assessment of future changes of heat stress in China in terms of the WBGT is necessary. Such an assessment could provide an overview of the different upper limits of human adaptation implied by different indices to the warming in future for China.

This study aims to investigate the future changes of extreme heat waves over China in the 21st century (particularly for 2020–50 and 2070–99). Heat waves characterized by both high temperature and heat stress in terms of WBGT in the two hottest months, i.e., July and August, are derived from the climate projections from five general circulation models (GCMs). Changes in the number of heat waves and their duration are expatiated, with the focus on presenting the characteristics of possible extreme heat waves in China under future climate change. This paper is organized as follows. Section 2 introduces the data and method used in this study. Section 3 provides the results, and conclusions and discussion are presented finally in Section 4.

2. Data and method

2.1 *Climatic data*

Daily temperature (average, maximum, and minimum) and relative humidity data over the period 1981–2099 are used in this study, which are derived from climate projections of five GCMs (Table 1) archived by the Coupled Model Intercomparison Project Phase 5 (CMIP5). The five GCMs are GFDL-ESM2M, HadGEM2-ES, IPSL-CM5A-LR, MIROC-ESM-CHEM, and NorESM1-M (Hempel et al., 2013). The climate projections are downscaled and provided by the Inter-Sectoral Impact Model Intercomparison Project (ISIMIP, https://www.isimip.org/) (Warszawski et al., 2014). The five GCMs were selected regarding the data availability and representativeness (Warszawski et al., 2014); they need to capture

Table 1. Five GCMs used in this study

GCM	Institution
GFDL-ESM2M	Geophysical Fluid Dynamics Laboratory, USA
HadGEM2-ES	Met Office Hadley Centre, UK
IPSL-CM5A-LR	Institut Pierre-Simon Laplace Climate Modelling Centre, France
MIROC-ESM-CHEM	Japan Agency for Marine–Earth Science and Technology, the Atmosphere and Ocean Research Institute at the University of Tokyo, and the National Institute for Environmental Studies, Japan
NorESM1-M	Norwegian Climate Centre, Norway

more than 70% of the full range of future projections of temperature changes (McSweeney and Jones, 2016). The five GCMs data were spatially interpolated and bias-corrected by using an observation-based dataset, the Water and Global Change (WATCH) forcing data (Weedon et al., 2011), to obtain projections with a finer spatial resolution of half a degree (Hempel et al., 2013).

These GCMs data have been used over the world in many studies on topics such as water scarcity assessment (Schewe et al., 2014), risk assessment for ecosystem shifts (Yin et al., 2016), and future projection of crop production (Elliott et al., 2014; Yin et al., 2015). For each GCM, two Representative Concentration Pathways (RCPs), i.e., the low mitigation scenario (RCP2.6) and the high baseline emission scenario (RCP8.5), are considered for representing the future climate change and bounding the uncertainties in climate projections associated with different RCPs. In addition, the China Meteorological Forcing Dataset (CMFD), provided by the Institute of Tibetan Plateau Research, Chinese Academy of Sciences (Yang et al., 2010; Chen et al., 2011; http://westdc.westgis.ac.cn/data/7a35329c-c53f-4267-aa07-e0037d913a21), are used for validation of the GCM-based temperature estimates.

2.2 *The wet-bulb globe temperature (WBGT)*

The concept of WBGT was initially proposed in the 1950s by the United States Army and Marine Corps, and is now the most widely used index of heat stress (Budd, 2008). When the WBGT is not available from observed wet-bulb, globe, and dry-bulb temperatures (American College of Sports Medicine (ACSM), 1984; Sherwood and Huber, 2010), the simplified WBGT is often used as an alternative to represent potential heat stress, as follows,

$$\mathrm{WBGT} = 0.567T + 0.393e_\mathrm{a} + 3.94, \tag{1}$$

where T (°C) is temperature and e_a (hPa) is simultaneous water vapor pressure. Equation (1) holds under moderately high radiation levels and light wind conditions. It may result in slight overestimation of heat stress in cloudy or windy conditions and during nighttime and early morning but underestimation during periods of full sun and small winds (Willett and Sherwood, 2012).

The daily maximum WBGT, defined as T_w, is derived from hourly WBGTs of each day based on the hourly temperature and water vapor pressure data. Hourly temperature is downscaled from daily maximum and minimum data using a cosine function (Debele et al., 2007):

$$T_i = T_\mathrm{av} + \frac{T_\mathrm{max} + T_\mathrm{min}}{2}\cos\left[\frac{\pi(t - t_\mathrm{x})}{12}\right], \tag{2}$$

where T_i is hourly temperature, t_x is the hour when the temperature is the highest in a day and is fixed at 1400 local time (i.e., 2 o'clock in the afternoon) in this study; T_av, T_max, and T_min are daily mean, maximum, and minimum temperature, respectively.

Daily water vapor pressure (e_a) is estimated by

$$e_\mathrm{a} = e_\mathrm{s}\frac{\mathrm{RH}}{100}, \tag{3}$$

where RH is relative humidity and e_s is saturated water vapor pressure estimated following Murray (1967):

$$e_\mathrm{s} = 6.108\exp\left(\frac{17.27T}{T + 237.3}\right). \tag{4}$$

Hourly water vapor pressure is derived from hourly dew point temperature by substituting T with hourly dew point temperature in Eq. (4). The hourly dew point temperature is estimated from daily minimum temperature following Debele et al. (2007). The diurnal cycle of water vapor pressures is then adjusted to have the same mean value as the daily water vapor pressure.

2.3 *Extreme high temperature and heat wave*

In this study, an extremely hot day is defined as days with daily maximum temperature (T_x) or T_w not less than 35°C, and the occurrence of a heat wave event is defined as three or more consecutive days with extremely high temperature, namely, T_x or $T_\mathrm{w} \geqslant 35$°C (China Meteorological Administration, 2015). However, it should be noted that T_x and T_w of 35°C may have different impacts on humans. When T_w is above 35°C, it would incur extreme risk to human health (Willett and Sherwood, 2012). The number of extreme hot days (NHD), number of heat waves (NHW), and mean duration per heat wave event (HWD) are estimated in each grid cell, and these values are subsequently domain-averaged for regional analyses. The NHD estimate denotes the sum of hot days during the two months (July and August) and the HWD estimate denotes the mean for all heat waves during the two months.

2.4 *Method*

For each RCP, T_x and T_w as well as the associated heat wave indicators, estimated as multimodel ensemble means from subsets of the five GCMs, are evaluated for three time periods: the baseline period (1981–2010), the near future (averages over the 2020–50 period, hereafter labeled as 2035), and the end of the century (averages over the 2070–99 period, hereafter labeled as 2085), respectively. Here, future changes are quantified as the differences between projections of future and the baseline periods. Eight regions over China (see Fig. 2) are defined

for the regional analysis.

3. Results

3.1 *Projected changes in high temperature*

Figure 1 shows the ensemble means of T_x and T_w from the GCMs over the baseline period (1981–2010), and the comparison with observation-based (CMFD) estimations (also see Liu et al., 2017). The GCM-based estimations resemble largely the CMFD-based ones with respect to their spatial patterns. In general, the historical mean T_x is high in Northwest and Southeast China and is the lowest over the Tibetan Plateau. The annual mean T_w in some southern parts of China exceeds 35°C and is higher than the corresponding T_x, but it is lower than T_x over the dry northern regions of China. This indicates that high temperature accompanied with wet weather tends to result in higher heat stress to humans. The differences between GCM-based and CMFD-based estimations are shown in Figs. 1e, f. Though the GCMs data were bias-corrected (Hempel et al., 2013), the GCMs generally overestimate T_x and T_w compared with the CMFD-based estimations for the baseline period, especially in western China (Figs. 1e, f) where caution should be given. Gauge stations are scarce in western China and it is often difficult to obtain high-quality large-scale observations there from observation-based spatial interpolation or reanalysis datasets (Zhang et al., 2014; Guo et al., 2016). It is also noted that T_w shows relatively less bias than T_x between GCM-based and CMFD-based estimations, which may be due to the fact that GCM projections of combined humidity and temperature could be more robust than temperature alone (Fischer and Knutti, 2013).

Figure 2 shows the means of T_x and T_w over the respective ensemble means of the changes across the five GCMs in 2035 and 2085 under RCP2.6 and RCP8.5. Compared with the baseline period, the future T_x and T_w are expected to increase by more than 1°C over China. Specifically, under the RCP2.6 scenario (Figs. 2c–f), by 2035, T_x (T_w) will increase by more than 1.5°C in considerable areas of China (mostly in East China), while in 2085, T_x (T_w) in most areas of China (in North and East China) will increase more than 1.5°C. For the RCP8.5 scenario, T_x and T_w changes in 2035 (Figs. 2g, h) generally resemble the 2085 counterparts under RCP2.6 (Figs. 2e, f), and in 2085, they will increase by more than 5°C across most parts of China. Particularly, over Northwest China, T_x will increase by more than 6°C (Fig. 2i).

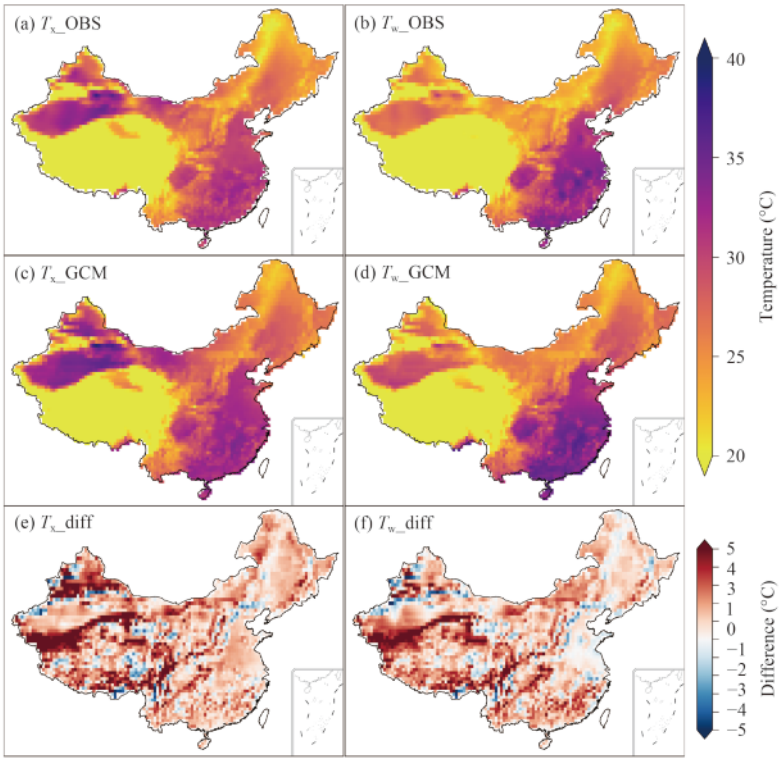

Fig. 1. (a, b) Observation-based estimations and (c, d) multimodel ensemble means of T_x and T_w over the baseline period (1981–2010), and (e, f) their respective differences between GCMs and observations. OBS: observation-based estimations; GCM: ensemble means from the five GCMs; and diff: differences between GCM and OBS.

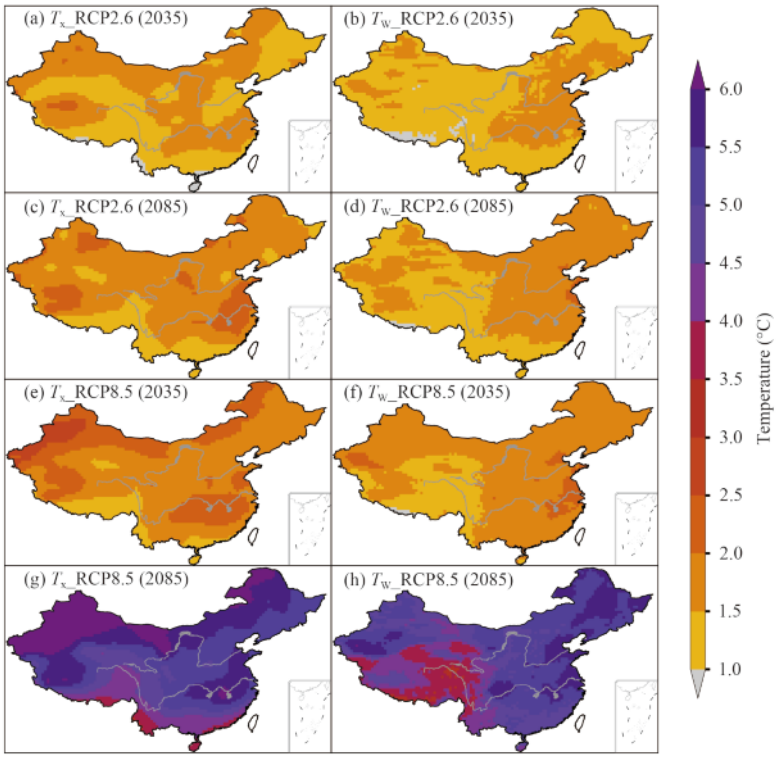

Fig. 2. The multimodel ensemble means of T_x and T_w for future periods (2035: the 2020–50 period, and 2085: the 2070–99 period) under (a–d) RCP2.6 and (e–h) RCP8.5.

It was noted that T_x and T_w in South and Southwest China generally show relatively small increases in the future in both scenarios.

Figure 3 shows histograms of annual values of grid-scale T_x and T_w for eight regions in China. For RCP2.6 (Fig. 3a), the histograms of T_x in 2035 and 2085 generally have very similar shapes but are shifted slightly rightward in comparison to those in the baseline period, which is likely because global warming will keep at a nearly constant level after the 2040s for this scenario (IPCC, 2013). The similar patterns are also found for T_w estimates. The differences between T_x and T_w histograms in the future resemble those in the baseline period, i.e., T_x histograms are usually at the right of T_w histograms over drier regions [western Northwest China (WNW) and eastern Northwest China (ENW)] while their relative positions are opposite in the relatively wet southern parts of China [Tibetan Plateau (TP), Southwest China (SW), South China (S), and East China (E)]. In Northeast China (NE), histograms of T_x and T_w are very close for both historical and future periods, while in North China (N), T_w is more frequent than T_x at low temperature (< 25°C) and very high temperature (> 30°C). Extreme T_x (> 35°C) in WNW and extreme T_w (> 35°C) in Southeast China (SE) will occur more frequently in the future. The histograms under the RCP8.5 scenario (Fig. 3b) present generally similar shapes with those of RCP2.6, but with larger rightward shifts relative to the baseline period, especially in 2085. Normal (i.e., most frequent) T_x in WNW and normal T_w in SE are much higher than 35°C in the future.

Figure 4 shows the temporal changes of domain-averaged T_x and T_w for the eight regions and entire China during 1981–2099 under the RCP2.6 and RCP8.5 scenarios. T_x and T_w generally keep increase and reach their peaks before the 2040s under RCP2.6, and dramatically increase over time and will reach as high as 40°C in SE under RCP8.5. The highest T_x and T_w in the future are generally found in SE. T_x in WNW will be as large as that in southeastern regions by the end of the century. Differences between T_x and T_w will slightly enlarge over time for most regions under both RCPs (also see Table 2). Obviously, the magnitude of T_x is higher than T_w over northern China, especially in WNW and ENW, while in TP, SW, S, and E, opposite patterns are shown (i.e., T_w is higher than T_x). In addition, the projected T_x is prone to larger model spreads (indicated by the standard deviations) than T_w, for example, in ENW, SW, and SE, and seems to show less uncertainties than T_w in WNW under the extremely dry climate there. It is noted that interannual variability of T_x is larger than that of T_w over all the regions.

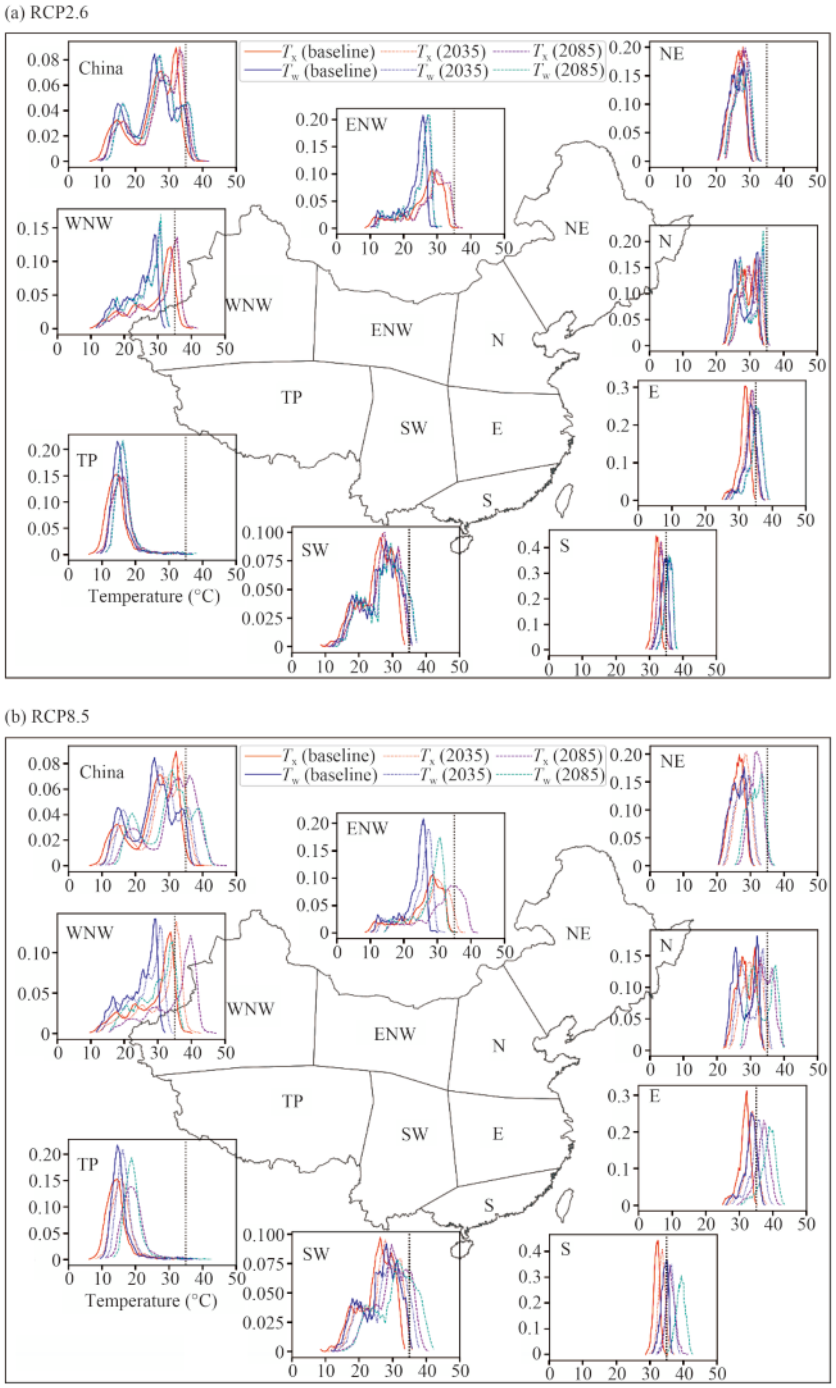

Fig. 3. The histograms (*x*-axis: temperature; *y*-axis: frequency of temperature) of T_x and T_w for different periods over eight regions of China under (a) RCP2.6 and (b) RCP8.5. The black dotted lines indicate the threshold of the extreme temperature of 35°C. WNW: western Northwest China; ENW: eastern Northwest China; N: North China; NE: Northeast China; TP: Tibetan Plateau; SW: Southwest China; E: East China; and S: South China.

3.2 *Projected changes of heat waves*

The performance of the GCMs in simulating summer heat waves over China is briefly evaluated by using the observation (CMFD)-based estimations. Figure 5 shows the domain-averaged T_x- and T_w-based NHD anomalies over the eight regions and entire China for the baseline period. The number of hot days (NHD) estimated from the GCMs and the CMFD are compared. In general, the annual NHD anomalies from GCMs are close to those from CMFD for many years, and the CMFD estimations show larger temporal variations than the GCM estimations for NHD values from both T_x and T_w. However, the

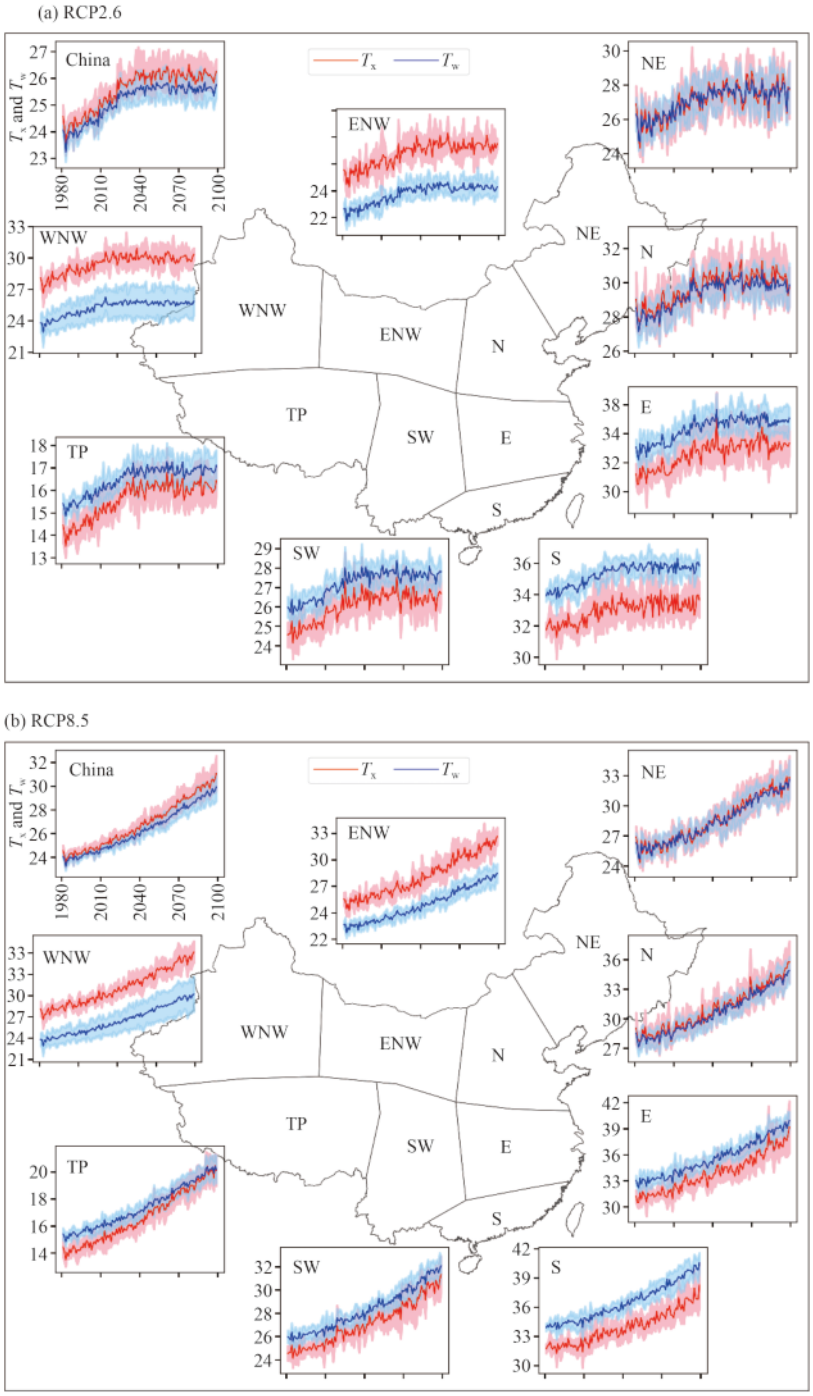

Fig. 4. Domain-averaged T_x and T_w in July and August over eight regions of China during 1981–2099 under (a) RCP2.6 and (b) RCP8.5. The lines denote the ensemble means and the shaded areas with light colors denote the spreads (standard deviations) across the five GCMs.

adjustment of variability is still a great challenge for bias-correction to GCM projections (Hempel et al., 2013). The CMFD and GCM estimations for NHD-T_w show relatively smaller differences than those for NHD-T_x over western China. The trends in NHDs are mostly captured by the GCM estimations, which are in favor of the assessment of the future heat waves in China over decades using the GCMs in the context of global warming.

Projected changes of the mean NHW over the future periods are shown in Fig. 6. In the baseline period, T_x-based mean NHW (NHW-T_x, Fig. 6a) is usually less than one per annum across a large portion of China. Note that obvious exceptions are found over parts of Southeast China and the northwestern Tarim basin, where the fre-

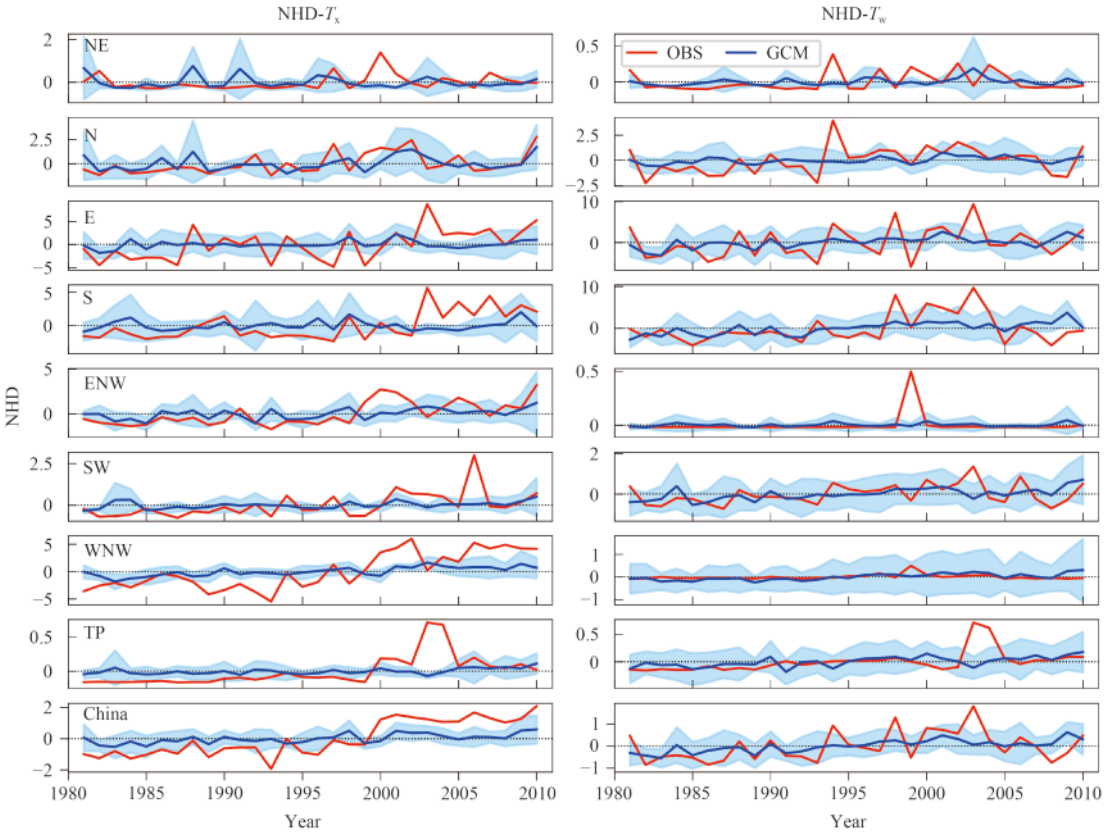

Fig. 5. Aggregated annual number of hot days (NHD) based T_x (NHD-T_x) and T_w (NHD-T_w) for regions and entire China. Red lines denote the NHDs estimated from the observational dataset (CMFD), and blue lines denote the GCM estimates. Light blue areas denote the spreads across GCMs.

quency of NHW-T_x is around or over two per annum. In contrast, the T_w-based heat wave (NHW-T_w, Fig. 6b) is primarily found in South and East China, whereas most areas of northern China, except for parts of the Tarim basin and Northeast China, are free of NHW-T_w.

The future projections indicate that NHW-T_x will increase over China (Figs. 6c, e, g), particularly in 2085 under RCP8.5, wherein NHW-T_x (Fig. 6i) is characterized by significant increases (more than two per annum) over many areas except for the Tarim basin. NHW-T_x will be above zero in the areas surrounding the Tibet where heat wave never occurs in the baseline period. In the future periods under RCP2.6 and RCP8.5 (Figs. 6d, f, h, j), with a few exceptions of decreases in South China, NHW-T_w changes are dominated by increases of less than two per annum, even over many northern regions where the T_w-based heat wave never occurs before. Particularly, under RCP8.5, NHW-T_w will decrease in considerable areas in South and East China in 2085 and increase more than two times over many other regions (Fig. 6j).

Figure 7 shows projected baseline and future changes of HWD. The T_x-based HWD (HWD-T_x, Fig. 7a) bears an overall resemblance with NHW-T_x (Fig. 6a), except for a small portion of Northeast China. The T_w-based HWD (HWD-T_w, Fig. 7b) in the baseline period is much longer (more than 10 days in some areas) in Southeast China than in the northern parts. Under RCP2.6, HWD-T_x will increase by one or less than one day per heat wave for most areas of China and decrease in Northeast China in 2035 and 2085 (Figs. 7c, e), while HWD-T_w will increase by several days (as many as 10 days in some areas) in Southeast China in 2035 and 2085 (Figs. 7d, f). Under RCP8.5, HWD-T_x and HWD-T_w in 2035 (Figs. 7g, h) tend to display similar spatial patterns to their counterparts in 2085 under RCP2.6 (i.e., Figs. 7e, f), while in 2085 (Figs. 7i, j), they show large increases over many areas, particularly over South China and the Tarim basin. In comparison to HWD-T_x, HWD-T_w shows a much larger increase in magnitude (more than 10 days) over many areas of Southeast China (Fig. 7j). The decrease of NHW-T_w (e.g., Fig. 6j) and significant increase of HWD-T_w (e.g., Fig. 7j) in Southeast China probably indicate an aggravation, rather than a mitigation, of heat stress over these areas.

The NHD estimated from T_x and T_w in the baseline

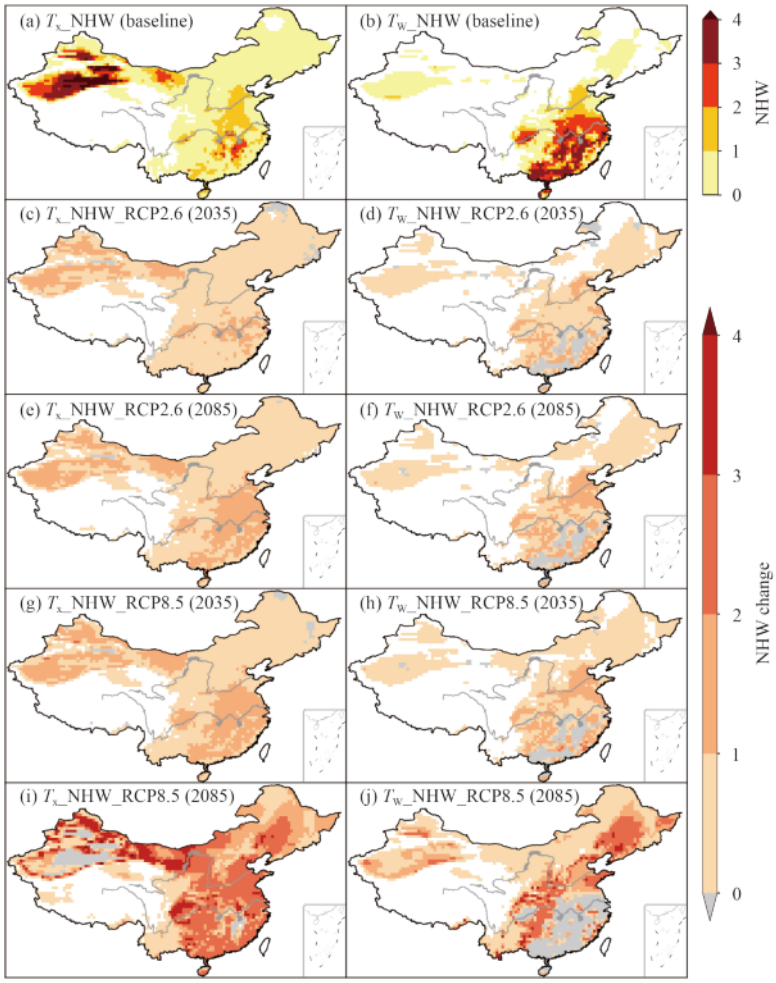

Fig. 6. The average number of T_x- (left panels) and T_w-based (right panels) heat wave (NHW) in China in the (a, b) baseline period and the future changes in 2035 and 2085 under (c–f) RCP2.6 and (g–j) RCP8.5. White color indicates no heat wave in the study area.

period and projected changes in future are shown in Fig. 8. The spatial pattern of NHD in the baseline period presents a well spatial correspondence with those of NHW (see Figs. 6a, b) and HWD (Figs. 7a, b); that is, large T_x- and T_w-based NHDs (NHD-T_x and NHD-T_w, respectively) are found in Northwest China (Southeast China). In future, the increase of annual mean NHD-T_x is mostly less than 15 days per annum in Northwest and Southeast China under RCP2.6, whereas NHD-T_w shows larger increases in Southeast China, with around 20 days per annum. As for the RCP8.5, NHD-T_x and NHD-T_w will increase by less than 20 days per annum in 2035 and nearly 30 days in 2085. Obviously, the increases in NHD-T_w are usually larger than that in NHD-T_x.

Figure 9 shows the temporal variation of spatially-averaged NHW and HWD over China. Overall, the variability of NHW-T_x and NHW-T_w under RCP2.6 (Fig. 9a) resembles that of corresponding temperatures of China (see Fig. 4a), showing that the NHWs increase and reach the peaks in the 2040s, with about 0.4 (0.1) times more NHW-T_x (NHW-T_w) per annum relative to the baseline period, and thereafter keep stable until the end of the century. HWD-T_w under RCP2.6 will increase by 2–4 days per annum after the 2040s, while HWD-T_x shows smaller increases of about 1 day per annum (Fig. 9c). Under RCP8.5, NHW-T_x and NHW-T_w both show remarkable linear trends over time. By the end of the century, the NHW-T_x will increase by more than one per annum, while the increase of NHW-T_x is less than 0.5 per annum (Fig. 9b). For the RCP8.5, both HWD-T_x and HWD-T_w show an increase with a rate of about 5 days per annum by the end of the century (Fig. 9d). It should be noted that HWD-T_w is much larger than HWD-T_x, which indicates that heat wave events defined by T_w will have longer spells and thus exert possible stronger heat stress to humans.

The temporal variations of NHW and HWD show clear spatial heterogeneity (Fig. 10). The increased NHW-T_x is found over all regions, particularly in Southeast China (SE) under RCP2.6 and in North and North-

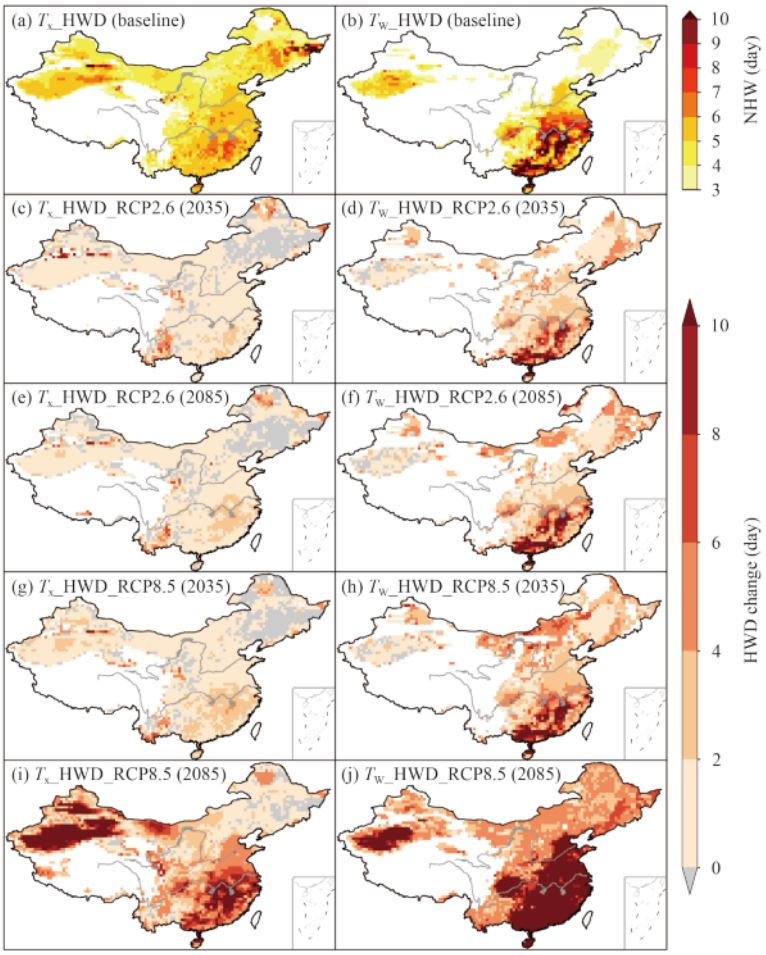

Fig. 7. Mean heat wave duration (HWD) based on T_x (left panels) and T_w (right panels) in China for the baseline period and their future changes in 2035 and 2085 under RCP2.6 and RCP8.5. White color indicates no heat wave in the study area.

east China under RCP8.5. Over many regions, NHW-T_x tends to show a larger increase than NHW-T_w. NHW-T_w often exhibits a small increase or even decreases in Southeast China and Tibet under RCP8.5. In Northeast (NE), North (N), and Southwest (SW) China, changes of NHW-T_x and NHW-T_w are very close under RCP2.6 and are slightly divergent by the end of the century under RCP8.5. For all the regions, NHW-T_x shows larger uncertainty across GCMs than NHW-T_w.

The increase of HWD-T_w will be higher than HWD-T_x in SE and Tibet under RCP2.6 and over most regions under RCP8.5 except for the NW (WNW and ENW), suggesting that heat waves based on T_w will be longer than those based on T_x in the future. The largest increase in HWD-T_w is found in South China (S) and followed by East China (E). In contrast, the changes in HWD-T_w and HWD-T_x are small over Northeast and Northwest China, as well as Tibet. HWD-T_w shows larger model spreads than HWD-T_x for all the regions.

3.3 *Uncertainties in temperature projections*

The T_w estimations from GCMs usually have lower uncertainties than T_x (Fig. 11), which is in line with previous results that uncertainties in the projections combining temperature and humidity are much smaller than those of the two individual variables from GCMs (Fischer and Knutti, 2013). The standard deviations (STDs) of T_w estimations across GCMs are smaller than those of T_x in 2035 and 2085 under both RCPs. Under RCP8.5, relatively high T_x uncertainties (over 1°C) mainly appear in South China and Tibet, as well as some areas of Northwest and Northeast China (2°C or more; Fig. 11d) in 2085. The STDs of T_w are small (less than 0.8°C) in most areas of China under RCP2.6 and are barely high in some areas where the T_x STDs are also high in 2085 under RCP8.5 (Fig. 11h).

Aggregated changes in T_x and T_w over regions and entire China for the two future periods are shown in Table 2. Compared to the baseline period, T_x of entire China will increase by about 1.5–1.9°C in 2035, and in-

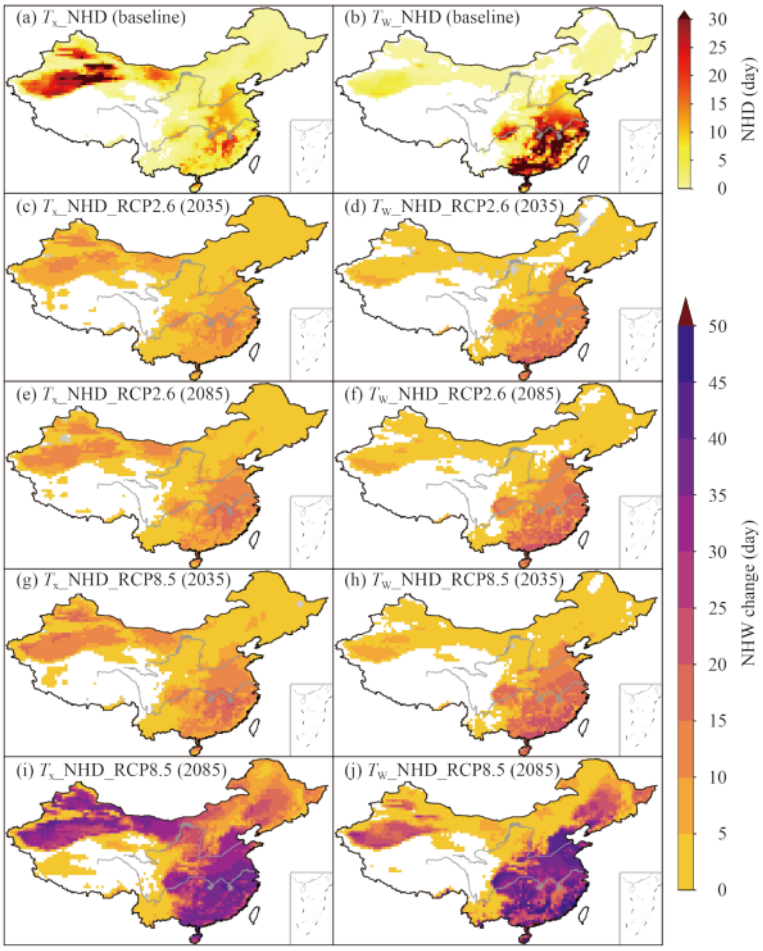

Fig. 8. The average number of extreme hot days (NHD) based on T_x (left panels) and T_w (right panels) in China for the baseline period and their future changes in 2035 and 2085 under RCP2.6 and RCP8.5.

crease by about 1.7–5.4°C in 2085, while T_w will increase by about 1.4–1.7°C in 2035 and by 1.5–4.9°C in 2085 across the scenarios. Changes in T_x (T_w) present significant spatial heterogeneity under both RCPs, with the range from 1.17 (1.2) to 2.21 (1.96) in 2035 and from 1.36 (1.33) to 6.34 (5.49) in 2085. The largest increase in T_x (T_w) mostly occurs in Northwest (North and Northeast) China. T_x and T_w in South China show the lowest increases in future, followed by those in Southwest China and Tibet. However, heat stress in South China indicated by T_w is expected to be the severest in terms of prolonged heat wave duration (see Figs. 7, 10). It is also noted that the future T_w shows smaller increases than T_x in most regions except for South China. Compared with T_w, T_x usually presents larger STD, which indicates lower model spreads in T_w projections (also see Figs. 4, 11).

4. Conclusions and discussion

Future changes of extreme heat events indicated by daily maximum temperature (T_x) and heat stress in terms of daily maximum wet-bulb globe temperature (T_w) in mainland China are investigated by using the climate projections from five GCMs under the RCP2.6 and RCP8.5 scenarios. The projected T_x tends to show a larger increase than T_w in the future. Specifically, T_x (T_w) will increase by 1.5–1.9°C (1.4–1.7°C) in 2035 and increase by 1.7–5.4°C (1.5–4.9°C) in 2085. In addition, the future changes of T_x and T_w are characterized by significant regional differences. T_x and T_w will dramatically increase by 5°C or more in many areas of China in 2085 under RCP8.5. The largest increases in T_x and T_w occur in Northwest China and the smallest increases occur in South and Southwest China.

Heat wave events and their characteristics, i.e., the number of extreme hot days (NHD), the number of heat waves (NHW), and the mean duration of individual heat waves (HWD), are estimated based on T_x and T_w. Under the RCP8.5 scenario, T_x- (T_w-) based heat waves will increase by more than 1 (nearly 0.5) per annum in the future across China, and the annual mean duration will in-

Table 2. Regional averages of changes in daily maximum temperature (T_x) and daily maximum WBGT (T_w), and their standard deviations (STD) for the 2020–50 (2035) period and the 2070–99 (2085) period

	RCP2.6				RCP8.5			
	T_x	STD	T_w	STD	T_x	STD	T_w	STD
2035								
China	1.52	0.68	1.41	0.51	1.90	0.73	1.73	0.53
NE	1.50	0.60	1.51	0.55	1.89	0.76	1.89	0.66
N	1.51	0.69	1.58	0.45	1.92	0.69	1.91	0.43
E	1.59	0.75	1.57	0.55	2.08	0.90	1.96	0.48
S	1.17	0.74	1.30	0.43	1.56	0.74	1.67	0.35
ENW	1.56	0.51	1.37	0.32	1.89	0.58	1.69	0.40
SW	1.47	0.78	1.36	0.53	1.79	0.55	1.65	0.33
WNW	1.65	0.58	1.43	0.47	2.21	0.70	1.78	0.54
TP	1.49	0.75	1.20	0.55	1.69	0.73	1.39	0.52
2085								
China	1.71	0.76	1.54	0.60	5.41	1.41	4.91	1.21
NE	1.68	0.80	1.67	0.70	5.64	1.42	5.49	1.26
N	1.85	0.79	1.76	0.51	5.44	1.14	5.36	0.91
E	1.93	0.88	1.74	0.60	5.50	1.32	5.38	1.04
S	1.36	0.62	1.44	0.40	4.20	0.94	4.85	0.86
ENW	1.81	0.52	1.53	0.45	5.66	1.09	4.77	0.94
SW	1.56	0.57	1.49	0.48	4.78	1.05	4.74	1.02
WNW	1.73	0.70	1.48	0.59	6.34	1.51	5.00	1.39
TP	1.66	0.88	1.33	0.64	4.89	1.29	4.03	1.00

NE: Northeast China; N: North China; E: East China; S: South China; ENW: eastern Northwest China; SW: Southwest China; WNW: western Northwest China; and TP: Tibetan Plateau.

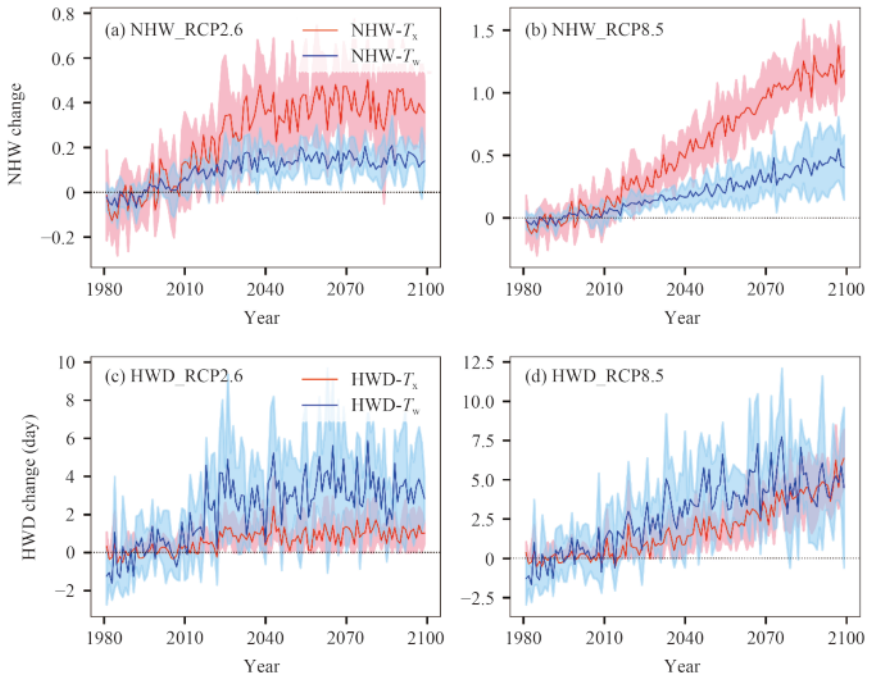

Fig. 9. Annual (a, b) NHW and (c, d) HWD changes in China with respect to the means of the baseline period (1981–2010) under (a, c) RCP2.6 and (b, d) RCP8.5. The lines denote the ensemble means and the areas with light colors denote the spreads (standard deviations) across the GCMs.

crease by around 5 days by the end of the century. The future changes of heat wave show considerable differences in Northwest and Southeast China. Relative to the baseline period, more extremely hot days (10–30 days) and longer heat wave durations (2–10 days) in future are expected to strike Northwest China, as well as Southeast China, where a large portion of China population is accommodated. T_w-based estimates, combining temperature and humidity, indicate more hot days and much longer heat waves than T_x in Southeast China. T_w projections also show less uncertainties compared to T_x projections, which is consistent with previous studies.

It has been reported that different indices may produce significant differences in identified heat waves dur-

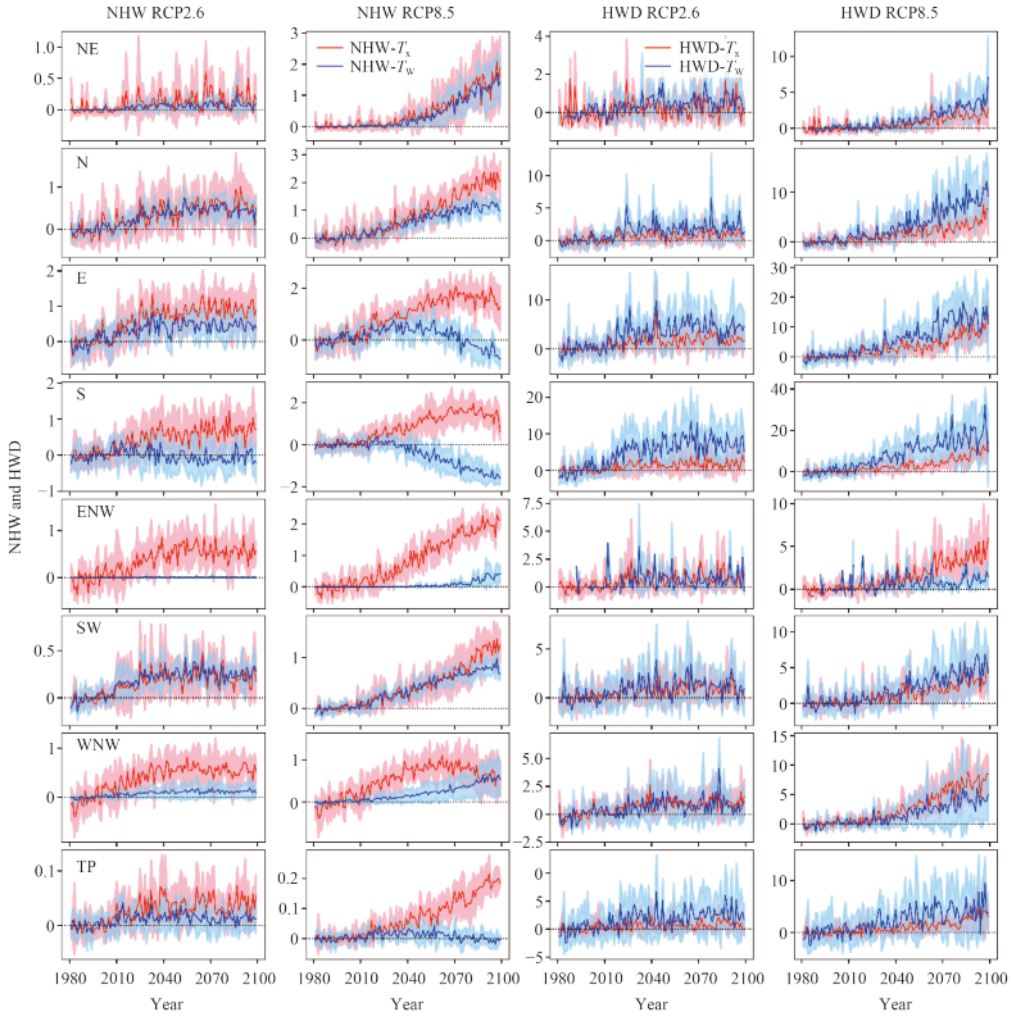

Fig. 10. Domain-averaged NHW and HWD changes relative to the baseline period (1981–2010) over eight regions of China under RCP2.6 and RCP8.5. The lines denote the multimodel ensemble means and the shaded areas with light colors denote the spreads (standard deviations) across the GCMs. The NHW and HWD changes are averaged over grid cells, excluding those cells without data (see Figs. 6, 7). The eight regions are shown in Fig. 3.

ing historical periods (Chen et al., 2015; Chen and Li, 2017; You et al., 2017). This study focuses on future projections of heat waves indicated by different definitions, and further highlights the discrepancies in heat wave estimates between those indices over China. The heat stress index WBGT, one of the heat wave indices used in this study, often indicates high heat stress that may narrow the adaptation limit to climate change (Sherwood and Huber, 2010). This study suggests that the more integrated index T_w could be a good alternative for heat stress assessment in China in future studies. Moreover, the likely aggravation of future heat stress indicated by T_x and T_w in Southeast China, the most developed area of China, raises an urgent need for adaptation measures.

The heat wave projections indicated by T_x in this study are consistent with previous studies (Guo et al., 2017), whereas the use of the WBGT here provides a new perspective and approach for heat wave assessment in mainland China. The simplified WBGT is a useful metric for heat stress perceived by humans because of its fairly good approximation to the heat stress that includes the effects of both temperature and other ambient conditions (Willett and Sherwood, 2012). Moreover, the relatively lower uncertainties in the WBGT projections across the GCMs make it a great potential for heat stress assessment under climate change.

It should be noted that WBGT was primarily developed and used by the US military; therefore, more local data in China are needed to establish the relationship between T_w and mortality (and morbidity) for further interpreting T_w and its impacts on human health. The fixed thresholds of T_w over different regions for the definition of heat waves may also result in under-/overestimation of health-related heat extremes (Li et al.,

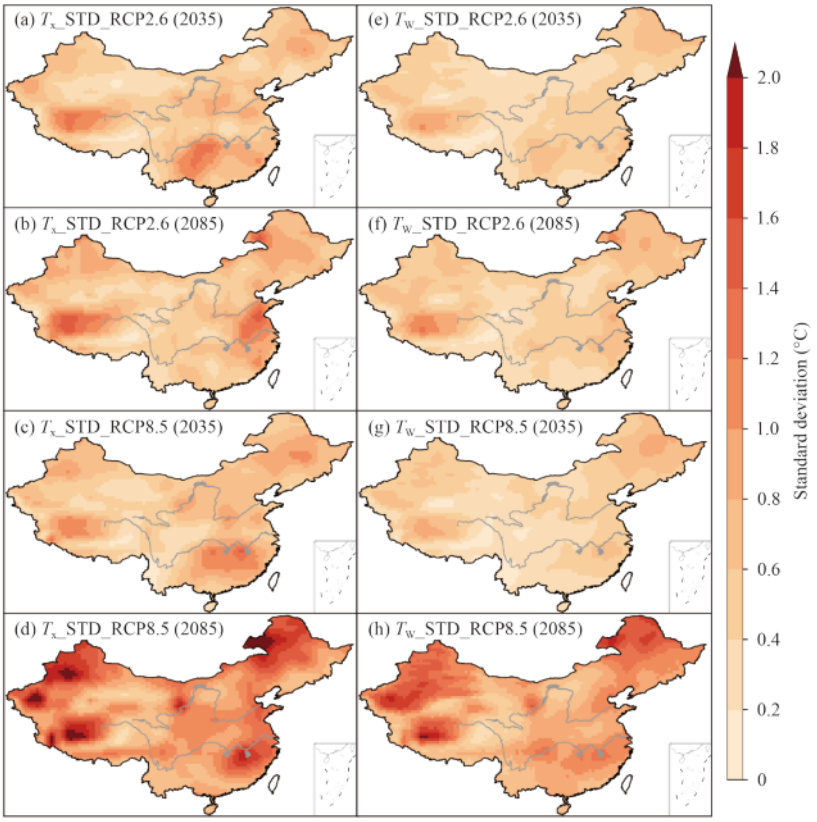

Fig. 11. Standard deviation (STD) of changes in (a–d) T_x and (e–h) T_w across the GCMs in 2035 and 2085 under (a, b, e, f) RCP2.6 and (c, d, g, h) RCP8.5.

2014). Both T_x and T_w estimates in western China should be treated with extreme caution since obvious biases are found over there, and further bias-correction of GCM data may be needed with more reliable large-scale observations in this region. In addition, the temporal downscaling of meteorological variables for WBGT calculation in this study may result in potential uncertainties in the WBGT estimates, which cannot be neglected in related health impact assessment.

This paper provides a preliminary assessment of extreme heat waves in mainland China in the future by integrating the effects of both temperature and humidity. Further research is needed to address potential health impact of projected heat waves by linking heat stress and human health (such as morbidity and mortality), which would benefit future heat wave projection and human adaptation. Literature studies have shown that anthropogenic influences would play an important role in increasing heat wave events (Herring et al., 2016; Sun et al., 2017). On the other hand, understanding of land–atmosphere coupling is also crucial for better projections of local heat waves in climate models (Seneviratne et al., 2010; Lorenz et al., 2016). Considerable evidence showed that changes of land surface fluxes and states were connected to (even remote) weather extremes (Hirschi et al., 2011; Zhang and Wu, 2011; Tang et al., 2014; Zhang et al., 2015). Further investigation into the form and evolution of heat waves, therefore, needs to focus on enhancing the forecasts of extreme heat waves by improving the related mechanism representation in climate models.

Acknowledgments. We acknowledge the Inter-Sectoral Impact Model Intercomparison Project (ISIMIP) coordination team for providing the bias-corrected GCM climate data (https://www.isimip.org/).

REFERENCES

American College of Sports Medicine (ACSM), 1984: Prevention of thermal injuries during distance running. *Phys. Sportsmed.*, **12**, 43–51, doi: 10.1080/00913847.1984.11701899.

Barriopedro, D., E. M. Fischer, and J. Luterbacher, 2011: The hot summer of 2010: Redrawing the temperature record map of Europe. *Science*, **332**, 220–224, doi: 10.1126/science.1201224.

Budd, G. M., 2008: Wet-bulb globe temperature (WBGT)—Its history and its limitations. *J. Sci. Med. Sport*, **11**, 20–32, doi: 10.1016/j.jsams.2007.07.003.

Chen, K., J. Bi, J. Chen, et al., 2015: Influence of heat wave definitions to the added effect of heat waves on daily mortality in Nanjing, China. *Sci. Total Environ.*, **506–507**, 18–25, doi:

10.1016/j.scitotenv.2014.10.092.

Chen, Y., and Y. Li, 2017: An inter-comparison of three heat wave types in China during 1961–2010: Observed basic features and linear trends. *Sci. Rep.*, **7**, 45619, doi: 10.1038/srep 45619.

Chen, Y. Y., K. Yang, J. He, et al., 2011: Improving land surface temperature modeling for dry land of China. *J. Geophys. Res.*, **116**, D20104, doi: 10.1029/2011JD015921.

China Meteorological Administration, 2015: QX/T 280–2015 Monitoring indices of high temperature extremes. Available at http://www.cmastd.cn/standardView.jspx?id=2103. Accessed on 26 March 2017. (in Chinese).

Debele, B., R. Srinivasan, and J. Y. Parlange, 2007: Accuracy evaluation of weather data generation and disaggregation methods at finer timescales. *Adv. Water Res.*, **30**, 1286–1300, doi: 10.1016/j.advwatres.2006.11.009.

Ding, T., and W. H. Qian, 2011: Geographical patterns and temporal variations of regional dry and wet heatwave events in China during 1960–2008. *Adv. Atmos. Sci.*, **28**, 322–337, doi: 10.1007/s00376-010-9236-7.

Elliott, J., D. Deryng, C. Müller, et al., 2014: Constraints and potentials of future irrigation water availability on agricultural production under climate change. *Proc. Natl. Acad. Sci. USA*, **111**, 3239–3244, doi: 10.1073/pnas.1222474110.

Fischer, E. M., and R. Knutti, 2013: Robust projections of combined humidity and temperature extremes. *Nat. Climate Change*, **3**, 126–130, doi: 10.1038/nclimate1682.

Grazzini, F., L. Ferranti, F. Lalaurette, et al., 2003: The exceptional warm anomalies of summer 2003. *ECMWF Newslett.*, **99**, 2–9.

Guo, X. J., J. B. Huang, Y. Luo, et al., 2017: Projection of heat waves over China for eight different global warming targets using 12 CMIP5 models. *Theor. Appl. Climatol.*, **128**, 507–522, doi: 10.1007/s00704-015-1718-1.

Guo, Y. J., S. Q. Zhang, J. H. Yan, et al., 2016: A comparison of atmospheric temperature over China between radiosonde observations and multiple reanalysis datasets. *J. Meteor. Res.*, **30**, 242–257, doi: 10.1007/s13351-016-5169-0.

Hauser, M., R. Orth, and S. I. Seneviratne, 2016: Role of soil moisture versus recent climate change for the 2010 heat wave in western Russia. *Geophys. Res. Lett.*, **43**, 2819–2826, doi: 10.1002/2016GL068036.

Hempel, S., K. Frieler, L. Warszawski, et al., 2013: A trend-preserving bias correction—the ISI-MIP approach. *Earth Syst. Dyn.*, **4**, 219–236, doi: 10.5194/esd-4-219-2013.

Herring, S. C., A. Hoell, M. P. Hoerling, et al., 2016: Explaining extreme events of 2015 from a climate perspective. *Bull. Amer. Meteor. Soc.*, **97**, S1–S145, doi: 10.1175/BAMS-ExplainingExtremeEvents2015.1.

Hirschi, M., S. I. Seneviratne, V. Alexandrov, et al., 2011: Observational evidence for soil-moisture impact on hot extremes in southeastern Europe. *Nat. Geosci.*, **4**, 17–21, doi: 10.1038/ngeo1032.

IPCC, 2013: *Climate Change 2013: The Physical Science Basis. Contribution of Working Group I to the Fifth Assessment Report of the Intergovernmental Panel on Climate Change*. T. F. Stocker, et al., Eds., Cambridge University Press, Cambridge, United Kingdom, New York, NY, USA, 1535 pp.

Leng, G. Y., Q. H. Tang, S. Z. Huang, et al., 2016: Assessments of joint hydrological extreme risks in a warming climate in China. *Int. J. Climatol.*, **36**, 1632–1642, doi: 10.1002/joc.4447.

Li, Y., Y. H. Ding, and W. J. Li, 2017: Observed trends in various aspects of compound heat waves across China from 1961 to 2015. *J. Meteor. Res.*, **31**, 455–467, doi: 10.1007/s13351-017-6150-2.

Li, Y. H., Y. B. Cheng, G. Q. Cui, et al., 2014: Association between high temperature and mortality in metropolitan areas of four cities in various climatic zones in China: A time-series study. *Environ. Health*, **13**, 65, doi: 10.1186/1476-069X-13-65.

Liu, X. C., Q. H. Tang, X. J. Zhang, et al., 2017: Spatially distinct effects of preceding precipitation on heat stress over eastern China. *Environ. Res. Lett.*, **12**, 115010, doi: 10.1088/1748-9326/aa88f8.

Lorenz, R., D. Argüeso, M. G. Donat, et al., 2016: Influence of land–atmosphere feedbacks on temperature and precipitation extremes in the GLACE-CMIP5 ensemble. *J. Geophys. Res.*, **121**, 607–623, doi: 10.1002/2015JD024053.

McSweeney, C. F., and R. G. Jones, 2016: How representative is the spread of climate projections from the 5 CMIP5 GCMs used in ISI-MIP? *Climate Serv.*, **1**, 24–29, doi: 10.1016/j.cliser.2016.02.001.

Miao, C. Y., Q. H. Sun, D. X. Kong, et al., 2016: Record-breaking heat in Northwest China in July 2015: Analysis of the severity and underlying causes. *Bull. Amer. Meteor. Soc.*, **97**, S97–S101, doi: 10.1175/BAMS-D-16-0142.1.

Mishra, V., A. R. Ganguly, B. Nijssen, et al., 2015: Changes in observed climate extremes in global urban areas. *Environ. Res. Lett.*, **10**, 024005, doi: 10.1088/1748-9326/10/2/024005.

Mitchell, D., 2016: Human influences on heat-related health indicators during the 2015 Egyptian heat wave. *Bull. Amer. Meteor. Soc.*, **97**, S70–S74, doi: 10.1175/BAMS-D-16-0132.1.

Mueller, B., X. B. Zhang, and F. W. Zwiers, 2016: Historically hottest summers projected to be the norm for more than half of the world's population within 20 years. *Environ. Res. Lett.*, **11**, 044011, doi: 10.1088/1748-9326/11/4/044011.

Murray, F. W., 1967: On the computation of saturation vapor pressure. *J. Appl. Meteor.*, **6**, 203–204, doi: 10.1175/1520-0450(1967)006<0203:otcosv>2.0.co;2.

Qi, L., and Y. Q. Wang, 2012: Changes in the observed trends in extreme temperatures over China around 1990. *J. Climate*, **25**, 5208–5222, doi: 10.1175/jcli-d-11-00437.1.

Schar, C., P. L. Vidale, D. Lüthi, et al., 2004: The role of increasing temperature variability in European summer heatwaves. *Nature*, **427**, 332–336, doi: 10.1038/nature02300.

Schewe, J., J. Heinke, D. Gerten, et al., 2014: Multimodel assessment of water scarcity under climate change. *Proc. Natl. Acad. Sci. USA*, **111**, 3245–3250, doi: 10.1073/pnas.1222460110.

Seneviratne, S. I., T. Corti, E. L. Davin, et al., 2010: Investigating soil moisture–climate interactions in a changing climate: A review. *Earth Sci. Rev.*, **99**, 125–161, doi: 10.1016/j.earscirev.2010.02.004.

Sherwood, S. C., and M. Huber, 2010: An adaptability limit to climate change due to heat stress. *Proc. Natl. Acad. Sci. USA*, **107**, 9552–9555, doi: 10.1073/pnas.0913352107.

Steadman, R. G., 1979: The assessment of sultriness. Part I: A

temperature–humidity index based on human physiology and clothing science. *J. Appl. Meteor.*, **18**, 861–873, doi: 10.1175/1520-0450(1979)018<0861:taospi>2.0.co;2.

Steadman, R. G., 1984: A universal scale of apparent temperature. *J. Climate Appl. Meteor.*, **23**, 1674–1687, doi: 10.1175/1520-0450(1984)023<1674:ausoat>2.0.co;2.

Sun, Q. H., C. Y. Miao, A. AghaKouchak, et al., 2017: Unraveling anthropogenic influence on the changing risk of heat waves in China. *Geophys. Res. Lett.*, **44**, 5078–5085, doi: 10.1002/2017GL073531.

Sun, Y., L. C. Song, H. Yin, et al., 2016: Human influence on the 2015 extreme high temperature events in western China. *Bull. Amer. Meteor. Soc.*, **97**, S102–S106, doi: 10.1175/bams-d-16-0158.1.

Sun, Y., X. B. Zhang, F. W. Zwiers, et al., 2014: Rapid increase in the risk of extreme summer heat in eastern China. *Nat. Climate Change*, **4**, 1082–1085, doi: 10.1038/nclimate2410.

Tang, Q. H., X. J. Zhang, and J. A. Francis, 2014: Extreme summer weather in northern mid-latitudes linked to a vanishing cryosphere. *Nat. Climate Change*, **4**, 45–50, doi: 10.1038/nclimate2065.

Wang, J. X. L., and D. J. Gaffen, 2001: Trends in extremes of surface humidity, temperature, and summertime heat stress in China. *Adv. Atmos. Sci.*, **18**, 742–751.

Warszawski, L., K. Frieler, V. Huber, et al., 2014: The Inter-Sectoral Impact Model Intercomparison Project (ISI-MIP): Project framework. *Proc. Nat. Acad. Sci. USA*, **111**, 3228–3232, doi: 10.1073/pnas.1312330110.

Weedon, G. P., S. Gomes, P. Viterbo, et al., 2011: Creation of the WATCH forcing data and its use to assess global and regional reference crop evaporation over land during the twentieth century. *J. Hydrometeor.*, **12**, 823–848, doi: 10.1175/2011jhm1369.1.

Wehner, M., D. Stone, H. Krishnan, et al., 2016: The deadly combination of heat and humidity in India and Pakistan in summer 2015. *Bull. Amer. Meteor. Soc.*, **97**, S81–S86, doi: 10.1175/BAMS-D-16-0145.1.

Willett, K. M., and S. Sherwood, 2012: Exceedance of heat index thresholds for 15 regions under a warming climate using the wet-bulb globe temperature. *Int. J. Climatol.*, **32**, 161–177, doi: 10.1002/joc.2257.

Yan, Z., P. D. Jones, T. D. Davies, et al., 2002: Trends of extreme temperatures in Europe and China based on daily observations. *Climatic Change*, **53**, 355–392, doi: 10.1023/A:1014939413284.

Yang, K., J. He, W. J. Tang, et al., 2010: On downward shortwave and longwave radiations over high altitude regions: Observation and modeling in the Tibetan Plateau. *Agric. For. Meteor.*, **150**, 38–46, doi: 10.1016/j.agrformet.2009.08.004.

Yin, Y., Q. Tang, and X. Liu, 2015: A multi-model analysis of change in potential yield of major crops in China under climate change. *Earth Syst. Dyn.*, **6**, 45–59, doi: 10.5194/esd-6-45-2015.

Yin, Y. Y., Q. H. Tang, L. X. Wang, et al., 2016: Risk and contributing factors of ecosystem shifts over naturally vegetated land under climate change in China. *Sci. Rep.*, **6**, 20905, doi: 10.1038/srep20905.

You, Q. L., J. Z. Min, K. Fraedrich, et al., 2014: Projected trends in mean, maximum, and minimum surface temperature in China from simulations. *Glob. Planet. Change*, **112**, 53–63, doi: 10.1016/j.gloplacha.2013.11.006.

You, Q. L., Z. H. Jiang, L. Kong, et al., 2017: A comparison of heat wave climatologies and trends in China based on multiple definitions. *Climate Dyn.*, **48**, 3975–3989, doi: 10.1007/s00382-016-3315-0.

Zhai, P. M., and X. H. Pan, 2003: Trends in temperature extremes during 1951–1999 in China. *Geophys. Res. Lett.*, **30**, 1913, doi: 10.1029/2003gl018004.

Zhang, J. Y., and L. Y. Wu, 2011: Land–atmosphere coupling amplifies hot extremes over China. *Chin. Sci. Bull.*, **56**, 3328–3332, doi: 10.1007/s11434-011-4628-3.

Zhang, Q., M. Z. Xiao, V. P. Singh, et al., 2015: Observational evidence of summer precipitation deficit-temperature coupling in China. *J. Geophys. Res.*, **120**, 10040–10049, doi: 10.1002/2015JD023830.

Zhang, X. J., Q. H. Tang, M. Pan, et al., 2014: A long-term land surface hydrologic fluxes and states dataset for China. *J. Hydrometeor.*, **15**, 2067–2084, doi: 10.1175/JHM-D-13-0170.1.

Zhang, Y. J., Z. Q. Gao, Z. T. Pan, et al., 2017: Spatiotemporal variability of extreme temperature frequency and amplitude in China. *Atmos. Res.*, **185**, 131–141, doi: 10.1016/j.atmosres.2016.10.018.

Tech & Copy Editor: Zhirong CHEN